

GTPC-SSCD: Gate-guided Two-level Perturbation Consistency-based Semi-Supervised Change Detection

Yan Xing¹, Qi'ao Xu^{2,3}, Zongyu Guo², Rui Huang^{2*}, Yuxiang Zhang²

¹College of Safety Science and Engineering, Civil Aviation University of China, Tianjin 300300, China

²College of Computer Science and Technology, Civil Aviation University of China, Tianjin 300300, China

³School of Computer Science and Technology, East China Normal University, Shanghai, 20062, China

Email: {yxing, 2021052074, 2022052044, rhuang, yxzhang}@cauc.edu.cn

Abstract—Semi-supervised change detection (SSCD) employs partially labeled data and a substantial amount of unlabeled data to identify differences between images captured in the same geographic area but at different times. However, existing consistency regularization-based SSCD methods only implement perturbations at a single level and can not exploit the full potential of unlabeled data. In this paper, we introduce a novel Gate-guided Two-level Perturbation Consistency regularization-based SSCD method (GTPC-SSCD), which simultaneously maintains strong-to-weak consistency at the image level and perturbation consistency at the feature level, thus effectively utilizing the unlabeled data. Moreover, a gate module is designed to evaluate the training complexity of different samples and determine the necessity of performing feature perturbations on each sample. This differential treatment enables the network to more effectively explore the potential of unlabeled data. Extensive experiments conducted on six public remote sensing change detection datasets demonstrate the superiority of our method over seven state-of-the-art SSCD methods.

Index Terms—Change detection (CD), consistency regularization, remote sensing, gate machine, semi-supervised learning

I. INTRODUCTION

Semi-supervised change detection (SSCD) aims to identify pixel-level changes between two images taken from the same scene at different times, using a limited amount of labeled data and a large amount of unlabeled data [1]–[3]. It has wide applications in various fields, including natural resource monitoring and utilization [4], [5], disaster monitoring and assessment [6], urban management and development [7], [8].

Semi-supervised methods can be divided into three categories: adversarial learning-based methods, pseudo-label-based methods, and consistency regularization-based methods. AdvEnt [9], SemiCDNet [10], and SALCD [11] are typical adversarial learning-based methods that employ alternative optimization strategies to improve the representation learning of their respective models. Pseudo-label-based methods, such as RC-CD [12], SemiSiROC [13], and DCF-CFe [14], emphasize the improvement of pseudo-label quality and apply some techniques to enhance feature distinctiveness. Consistency regularization-based methods, including SemiCD [15], SemiSANet [16], Semi-LCD [17], SemiBuildingChange [18],

This work was supported in part by the Scientific Research Program of Tianjin Municipal Education Commission under Grant 2023KJ232. (Corresponding author: Rui Huang.)

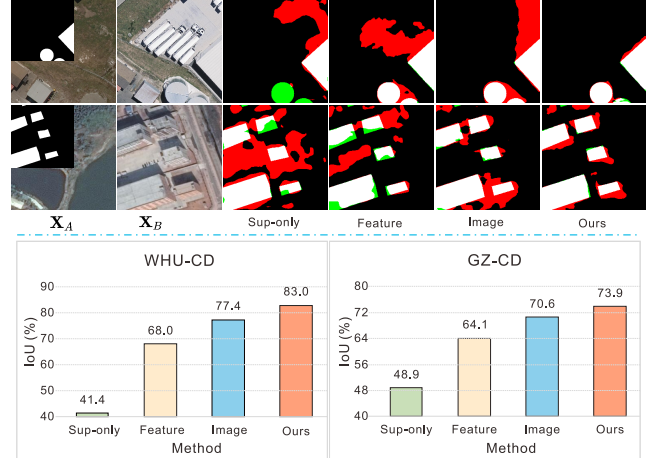


Fig. 1. Motivation: Comparison of SSCD with different perturbations by 5% labeled training data. Sup-only denotes that our method only be trained by labeled training data. Feature: Feature-level perturbation consistency method. Image: Image-level strong-to-weak consistency method. Different colors are used for a better view, i.e., white for true positive, black for true negative, red for false positive, and green for false negative.

and SemiPTCD [19], enforce that perturbed images or features produce identical outputs as the original inputs [20].

Recently, the consistency regularization-based framework have been increasingly drawn to SSCD methods for its simplicity and stability. However, current methods often modify network architectures or introduce additional information based on image-level weak-to-strong consistency. For example, SemiSANet [16] constructs a siamese nested UNet with graph attention, while MTCNet [21] adds extra segmentation labels to change labels. ST-RCL [22] combines self-training and consistency learning for SSCD. Concurrently, feature-level consistency regularization remains relatively simplistic and underdeveloped, such as UniMatch's implementation of a dropout to enforce feature consistency [23]. Thus, there exists significant potential in integrating image-level and feature-level consistency regularization to further enhance the performance and robustness of SSCD.

Our research shows that employing a simple SSCD architecture and applying perturbations either at the image or feature level does not yield satisfactory performance. Fig. 1 presents the results of SSCD networks employing perturba-

tions at different perspectives with a ratio of 5% labeled data and 95% unlabeled data on two CD datasets [10], [24]. Although perturbations contribute to enhancing model robustness, relying solely on image perturbations may affect pixel integrity and segmentation, and exclusive dependence on feature perturbations might struggle with image diversity.

In this paper, we explore consistency regularization at a broader scope and propose a Gate-guided Two-level Perturbation Consistency regularization-based SSCD method (GTPC-SSCD). By learning both image-level strong-to-weak consistency and feature-level perturbation consistency, our method can benefit from a more thorough comprehension of the data, leading to improved robustness and discriminability. Furthermore, performing the same treatment on all samples constrains the potential effectiveness of perturbation, particularly evident in remote sensing change detection scenarios. To tackle this issue, we develop a gate module to distinguish the difficulty of training samples and determine the application of feature perturbation accordingly. As presented in Fig. 1, the performance of our method is superior to other three methods. Our contributions are summarized as follows:

- We separately analyze image and feature perturbation implementations in SSCD, and meticulously combine them with optimized strategies to improve performance.
- We introduce a gate-guided two-level perturbation consistency regularization-based SSCD method, utilizing a gate mechanism to assess the difficulty of samples and decide whether to apply feature perturbations.
- We conduct extensive experiments on six public CD datasets. Our method exhibits higher accuracy compared to other seven state-of-the-art SSCD methods.

II. METHODOLOGY

Semi-supervised change detection (SSCD) utilizes a limited amount of labeled data and a large amount of unlabeled data to train a change detection network for accurate change map generation. The training set consists of two subsets, a labeled set and an unlabeled set. The labeled set can be represented as $\mathcal{D}_l = \{(\mathbf{X}_{A,i}^l, \mathbf{X}_{B,i}^l), \mathbf{Y}_i^l\}_{i=1}^M$, where $(\mathbf{X}_{A,i}^l, \mathbf{X}_{B,i}^l)$ denotes the i -th labeled image pair, $\mathbf{X}_{A,i}^l$ is the pre-change image, $\mathbf{X}_{B,i}^l$ is the post-change image, and \mathbf{Y}_i^l is the corresponding ground truth. Let $\mathcal{D}_u = \{(\mathbf{X}_{A,i}^u, \mathbf{X}_{B,i}^u)\}_{i=1}^N$ denotes the unlabeled set. $(\mathbf{X}_{A,i}^u, \mathbf{X}_{B,i}^u)$ is the i -th unlabeled image pair. M and N indicate the number of labeled and unlabeled image pairs, respectively. In most cases, we have $N \gg M$. In the following sections, we will introduce the implementation details of the proposed change detection network.

A. Our consistency regularization-based SSCD method

Our SSCD method consists of a supervised training part and an unsupervised training part.

In the supervised training part, we use the labeled set \mathcal{D}_l to train the CD network ϕ . The network processes weakly augmented image pairs to generate change map \mathbf{P}^l . We apply

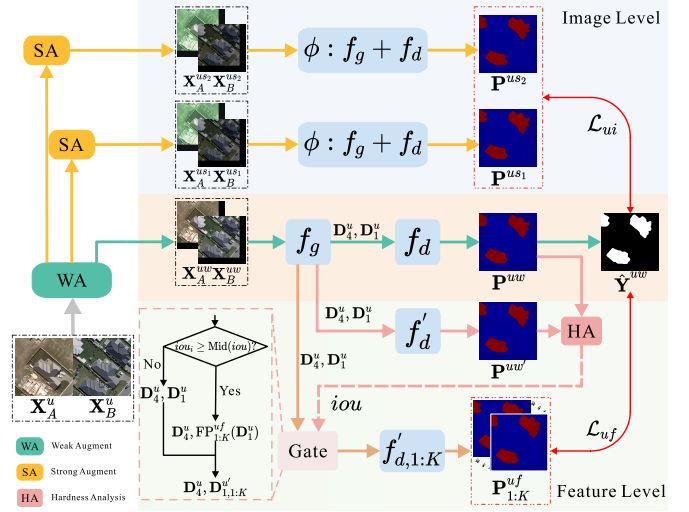


Fig. 2. Framework of the proposed GTPC-SSCD method.

standard cross-entropy (CE) loss as supervision. The loss of the supervised training part is:

$$\mathcal{L}_s = \mathcal{L}_{CE}(\mathbf{P}^l, \mathbf{Y}^l). \quad (1)$$

The unsupervised part is illustrated in Fig. 2, we apply two-level perturbations to train ϕ on the unlabeled set \mathcal{D}_u . Specifically, we exploit strong-to-weak consistency at the image level and perturbation consistency at the feature level. The former enhances the model's robustness to various data transformations, while the latter improves the model's generalization ability and resistance to interference.

Strong-to-weak consistency learning. Drawing inspiration from ConMatch [25] and ReMixMatch [26], we increase the number of strong augmentation branches and ensure the strong-to-weak consistency, fully maximizing the benefits of strong augmentation. Specifically, we apply two independent strong augmentations on $(\mathbf{X}_A^{uw}, \mathbf{X}_B^{uw})$, resulting in $(\mathbf{X}_A^{us1}, \mathbf{X}_B^{us1})$ and $(\mathbf{X}_A^{us2}, \mathbf{X}_B^{us2})$. They are fed into ϕ and generate three change maps \mathbf{P}^{uw} , \mathbf{P}^{us1} and \mathbf{P}^{us2} .

We use \mathbf{P}^{uw} to generate pseudo-label $\hat{\mathbf{Y}}^{uw}$ by:

$$\hat{\mathbf{Y}}^{uw} = \begin{cases} 1, & \text{if } \mathbf{P}^{uw} > \tau \\ 0, & \text{else} \end{cases} \quad (2)$$

where $\tau = 0.95$ is a confidence threshold. The image-level consistency loss of the unsupervised part is as:

$$\mathcal{L}_{ui} = \frac{1}{2}(\mathcal{L}_{CE}(\mathbf{P}^{us1}, \hat{\mathbf{Y}}^{uw}) + \mathcal{L}_{CE}(\mathbf{P}^{us2}, \hat{\mathbf{Y}}^{uw})). \quad (3)$$

In our experiments, weak augmentations consist of random resizing, cropping, and random horizontal flipping. Strong augmentations include random color jittering, Gaussian blur, and CutMix [27].

Perturbation consistency learning. We introduce feature-level consistency by applying several different perturbations on change features and enforcing the perturbation consistency. The process of generating change maps $\mathbf{P}_{1:K}^{uf}$ is depicted as:

$$\mathbf{P}_{1:K}^{uf} = f_{d,1:K}'(\mathbf{D}_4^u, \mathbf{D}_{1:K}^{u'}), \quad (4)$$

where $\mathbf{D}_{1:K}^{u'} = \{\mathbf{D}_{1,k}^{u'}\}_{k=1}^K$, represents the difference features after perturbation. $f_{d,1:K}' = \{f_{d,k}'\}_{k=1}^K$, denotes the auxiliary decoders. $\mathbf{P}_{1:K}^{uf} = \{\mathbf{P}_k^{uf}\}_{k=1}^K$. The feature-level consistency loss \mathcal{L}_{uf} is expressed as:

$$\mathcal{L}_{uf} = \frac{1}{K} \sum_{k=1}^K \mathcal{L}_{CE}(\mathbf{P}_k^{uf}, \hat{\mathbf{Y}}^{uw}), \quad (5)$$

where K is the total number of the auxiliary decoders. We apply seven types of feature perturbations [28], i.e., feature noise, feature dropout, object masking, context masking, guided cutout, Intermediate VAT [29], and random dropout.

Hardness analysis based gate mechanism. We add an additional decoder to produce $\mathbf{P}_i^{uw'}$ and conduct an Intersection over Union (IoU) comparison with \mathbf{P}_i^{uw} to assess the complexity of each sample. Utilizing a gate mechanism, we select challenging samples and apply various perturbations on \mathbf{D}_1^u of these selected samples to obtain perturbed features. The process can be formulated as:

$$iou_i = \text{IoU}(\mathbf{P}_i^{uw'}, \mathbf{P}_i^{uw}), \quad (6)$$

$$\mathbf{D}_{1:K}^{u'} = \begin{cases} \text{FP}_{1:K}(\mathbf{D}_1^u), & \text{if } iou_i \geq \text{Mid}(iou) \\ \mathbf{D}_1^u, & \text{else} \end{cases} \quad (7)$$

where iou_i represents the IoU score of the i -th sample, $\text{Mid}(iou)$ is the median IoU score. $\text{FP}_{1:K}(\cdot)$ denotes K different perturbations to the input features, respectively.

Loss function. The total loss consists of the supervised loss \mathcal{L}_s , the image-level consistency loss \mathcal{L}_{ui} and the feature-level consistency loss \mathcal{L}_{uf} . It can be expressed as:

$$\mathcal{L} = \lambda_1 \mathcal{L}_s + \lambda_2 \mathcal{L}_{ui} + \lambda_3 \mathcal{L}_{uf}, \quad (8)$$

where $\lambda_1 = 0.5$, $\lambda_2 = 0.25$, and $\lambda_3 = 0.25$.

B. Implementation detail

1) *Change Detection Network:* Our CD network ϕ consists of two components: a difference feature generator f_g and a decoder f_d . The process of generating change map \mathbf{P} is simply expressed by:

$$\mathbf{P} = \phi(\mathbf{X}_A, \mathbf{X}_B) = f_d(f_g(\mathbf{X}_A, \mathbf{X}_B)). \quad (9)$$

Difference feature generator. The feature encoder is built on ResNet50 [30] with a siamese setup. Deep features contain rich semantic information, while shallow features encompass abundant details. We use the features of the first and fourth residual modules to calculate the difference features \mathbf{D}_i by:

$$\mathbf{D}_i = |\mathbf{C}_i^A - \mathbf{C}_i^B|, i = 1, 4, \quad (10)$$

where \mathbf{C}_i^A and \mathbf{C}_i^B are the features of the i -th residual module from \mathbf{X}_A and \mathbf{X}_B , respectively. $|\cdot|$ is the absolute operation.

Decoder. The decoder is used to process change features and generate change maps. We apply an Atrous Spatial Pyramid Pooling (ASPP) [31] on \mathbf{D}_4 to obtain richer information \mathbf{F}_4 . Next, we combine \mathbf{D}_1 and the upsampled feature of \mathbf{F}_4

and employ a classifier to generate \mathbf{P} . The process can be formulated as:

$$\mathbf{F}_4 = \text{ASPP}(\mathbf{D}_4), \quad (11)$$

$$\mathbf{F}_1 = \text{CBR}_3(\text{CBR}_3([\text{Up}(\mathbf{F}_4), \text{CBR}_1(\mathbf{D}_1)])), \quad (12)$$

$$\mathbf{P} = \text{Conv}_1(\mathbf{F}_1), \quad (13)$$

where $\text{ASPP}(\cdot)$ denotes the ASPP process, $\text{Up}(\cdot)$ is upsampling operation, $[\cdot, \cdot]$ denotes concatenate operation. $\text{CBR}_k(\cdot)$ denotes a $k \times k$ convolutional layer followed with Batch Normalization and ReLU, and $\text{Conv}_1(\cdot)$ represents a 1×1 convolutional layer.

2) *Super-parameters:* We use PyTorch to conduct experiments on an NVIDIA RTX2080Ti GPU. Our model adopts the SGD optimizer with learning rate of 0.02, momentum of 0.9, and weight decay of $1e-4$, respectively. All models are trained for 80 epochs with batch size of 4 for both labeled and unlabeled data.

III. EXPERIMENTS

A. Experimental Setups

Baselines. We compare the proposed method with seven existing state-of-the-art methods, including AdvEnt [9], s4GAN [32], SemiCDNet [10], SemiCD [15], RC-CD [12], SemiPTCD [19], and UniMatch [23]. Sup-only refers to our method that exclusively utilizes labeled data for training.

Datasets. We conduct experiments on six widely used remote sensing CD datasets, namely WHU-CD [24], LEVIR-CD [7], BCD [24], GZ-CD [10], EGY-BCD [33], and CDD [34]. Table I details our datasets, including number of image pairs, image size, train/val/test splits, spatial resolution, and change types. The first five CD datasets mainly focus on building changes, while the last CD dataset consists of multiple types of changes, including buildings, vehicles, road expansions, and more. All images are cropped into non-overlapping patches of size 256×256 , which are then divided into training, validation, and test sets. The training set is further divided into labeled and unlabeled data with the following ratios: [5%, 95%], [10%, 90%], [20%, 80%], [40%, 60%].

Criterion. Following Bandara *et al.* [15], Mao *et al.* [19], and Yang *et al.* [23], we adopt intersection over union (IoU) and overall accuracy (OA) as the primary performance metric to evaluate different change detection methods.

B. Results and Discussion

Comparison to the State-of-the-Art. Table II exhibits the quantitative results of different methods on WHU-CD, LEVIR-CD, BCD, GZ-CD, EGY-BCD, and CDD datasets. From the findings in these tables, we can draw the following observations. ❶ Most SSCD methods outperform Sup-only under the same partition, confirming the benefit of unlabeled data for SSCD. ❷ Our method achieves the best performance across all four partitions, notably surpassing other methods, especially on WHU-CD and GZ-CD. On WHU-CD, compared to the current SOTA method UniMatch, our method brings 4.3%, 3.2%, 3.0%, and 1.7% performance gain in terms of IoU with 5%, 10%, 20%, and 40% labeled training data,

TABLE I
DATASET DETAILS.

Dataset	Image pairs	Image size	Train/Val/Test	Spatial resolution	Changes
WHU-CD	1	15354 × 32507 × 3	5974/743/744	0.2 m/pixel	building
LEVIR-CD	637	1024 × 1024 × 3	7120/1024/2048	0.5 m/pixel	building
BCD	1922	256 × 256 × 3	1538/192/192	0.2 m/pixel	building
GZ-CD	19	1006 × 1168 × 3, 4936 × 5224 × 3	2882/360/361	0.55 m/pixel	building
EGY-BCD	6091	256 × 256 × 3	4264/1218/609	0.25 m/pixel	building
CDD	16000	256 × 256 × 3	10000/3000/3000	0.03-1 m/pixel	building, car, tree, road, <i>etc.</i>

TABLE II
QUANTITATIVE COMPARISON OF DIFFERENT METHODS ON SIX CD DATASETS. THE HIGHEST SCORES ARE MARKED IN **BOLD**.

Method	WHU-CD								LEVIR-CD							
	5%		10%		20%		40%		5%		10%		20%		40%	
	IoU	OA	IoU	OA	IoU	OA	IoU	OA	IoU	OA	IoU	OA	IoU	OA	IoU	OA
AdvEnt [9]	57.7	97.87	60.5	97.79	69.5	98.50	76.0	98.91	67.1	98.15	70.8	98.38	74.3	98.59	75.9	98.67
s4GAN [32]	57.3	97.94	58.0	97.81	67.0	98.41	74.3	98.85	66.6	98.16	72.2	98.48	75.1	98.63	76.2	98.68
SemiCDNet [10]	56.2	97.78	60.3	98.02	69.1	98.47	70.5	98.59	67.4	98.11	71.5	98.42	74.9	98.58	75.5	98.63
SemiCD [15]	65.8	98.37	68.0	98.45	74.6	98.83	78.0	99.01	74.2	98.59	77.1	98.74	77.9	98.79	79.0	98.84
RC-CD [12]	58.0	98.01	61.7	98.00	74.0	98.83	73.9	98.85	74.0	98.52	76.1	98.65	77.1	98.70	77.6	98.72
SemiPTCD [19]	74.1	98.85	74.2	98.86	76.9	98.95	80.8	99.17	71.2	98.39	75.9	98.65	76.6	98.65	77.2	98.74
UniMatch [23]	78.7	99.11	79.6	99.11	81.2	99.18	83.7	99.29	82.1	99.03	82.8	99.07	82.9	99.07	83.0	99.08
Sup-only	41.4	96.36	55.0	97.28	49.3	96.98	65.6	98.26	71.8	98.46	78.0	98.78	77.7	98.76	78.9	98.83
Ours	83.0	99.30	82.8	99.28	84.2	99.31	85.4	99.37	83.2	99.09	83.1	99.08	83.7	99.12	83.5	99.10
	BCD								GZ-CD							
AdvEnt [9]	62.4	91.93	69.1	93.29	75.2	94.85	77.1	95.14	56.7	95.52	57.5	95.99	70.3	97.28	70.8	97.29
s4GAN [32]	57.7	90.77	70.9	93.95	74.9	94.64	78.0	95.35	59.4	96.13	61.6	96.23	68.5	97.10	69.4	97.08
SemiCDNet [10]	59.4	91.49	70.3	93.83	74.4	94.65	77.7	95.33	57.9	95.38	54.9	95.52	68.9	97.16	69.7	97.20
SemiCD [15]	60.9	92.08	73.1	94.23	77.5	95.26	79.3	95.66	59.5	96.27	58.6	96.03	67.0	97.03	71.5	97.36
RC-CD [12]	75.4	94.79	77.7	95.18	79.7	95.77	80.6	95.95	62.2	96.26	63.9	96.55	74.1	97.69	74.2	97.57
UniMatch [23]	78.3	96.17	79.9	96.48	80.7	96.58	81.7	96.79	68.7	97.06	69.5	97.41	72.8	97.71	71.1	97.48
Sup-only	59.3	91.49	63.3	92.48	74.1	95.16	70.1	95.16	48.9	94.49	36.9	91.94	53.5	95.44	54.4	95.73
Ours	79.9	96.52	81.3	96.76	81.3	96.78	82.4	96.95	73.9	97.71	70.7	97.36	77.8	98.09	78.4	98.17
	EGY-BCD								CDD							
AdvEnt [9]	52.0	95.30	58.1	96.26	59.8	96.46	63.8	96.94	63.8	94.98	72.7	96.32	79.0	97.22	82.8	97.72
s4GAN [32]	53.2	95.62	56.5	96.26	59.4	96.62	64.1	96.83	62.5	94.92	70.4	96.12	78.7	97.20	82.8	97.72
SemiCDNet [10]	52.7	95.36	56.9	96.02	59.8	96.53	63.6	96.96	64.3	95.01	72.5	95.88	79.1	97.23	82.6	97.73
SemiCD [15]	54.3	95.79	59.2	96.29	61.8	96.61	65.4	96.96	66.4	95.39	74.9	96.71	81.2	97.54	84.4	97.93
RC-CD [12]	59.0	96.17	61.6	96.51	64.6	96.79	67.7	97.09	69.2	95.82	73.4	96.29	80.1	97.32	82.7	97.67
UniMatch [23]	62.8	96.74	65.5	97.10	63.6	96.91	67.3	97.26	74.8	96.69	80.3	97.41	86.8	98.30	90.7	98.81
Sup-only	44.5	94.03	54.9	95.65	44.8	94.28	60.0	96.37	49.7	92.58	62.3	94.71	66.2	95.32	78.5	97.15
Ours	64.5	96.91	65.9	97.15	66.1	97.13	68.9	97.44	76.4	96.89	82.3	97.70	88.0	98.46	90.2	98.74

respectively. On GZ-CD, the improved performance with IoU of our method over the best UniMatch are 5.2%, 1.2%, 5.0%, and 7.3%.

Detection results. Fig. 3 shows some examples of different methods on six CD datasets under the partition of 5%. Our method exhibits higher accuracy and richer details. Both quantitative and qualitative results support our method’s superiority.

Computational complexity analysis. Table III shows a detailed comparison of parameters and computation costs of different methods. Compared to other methods, our method achieves a high FPS with a moderate parameter count, striking an effective balance between performance and efficiency.

Ablation study. Table IV illustrates four sets of abla-

TABLE III
COMPARISON OF PARAMETERS AND COMPUTATIONAL COSTS OF DIFFERENT METHODS.

Method	GFLOPs	Params (M)	FPS
AdvEnt	74.06	49.6	40.82
s4GAN	76.72	49.6	41.54
SemiCDNet	75.69	52.4	40.87
SemiCD	75.37	50.7	39.30
UniMatch	38.30	40.5	52.19
Ours	65.87	57.3	51.64

tion studies. From this table, we have the following findings. ① Under the “Without Gate” condition, both image-

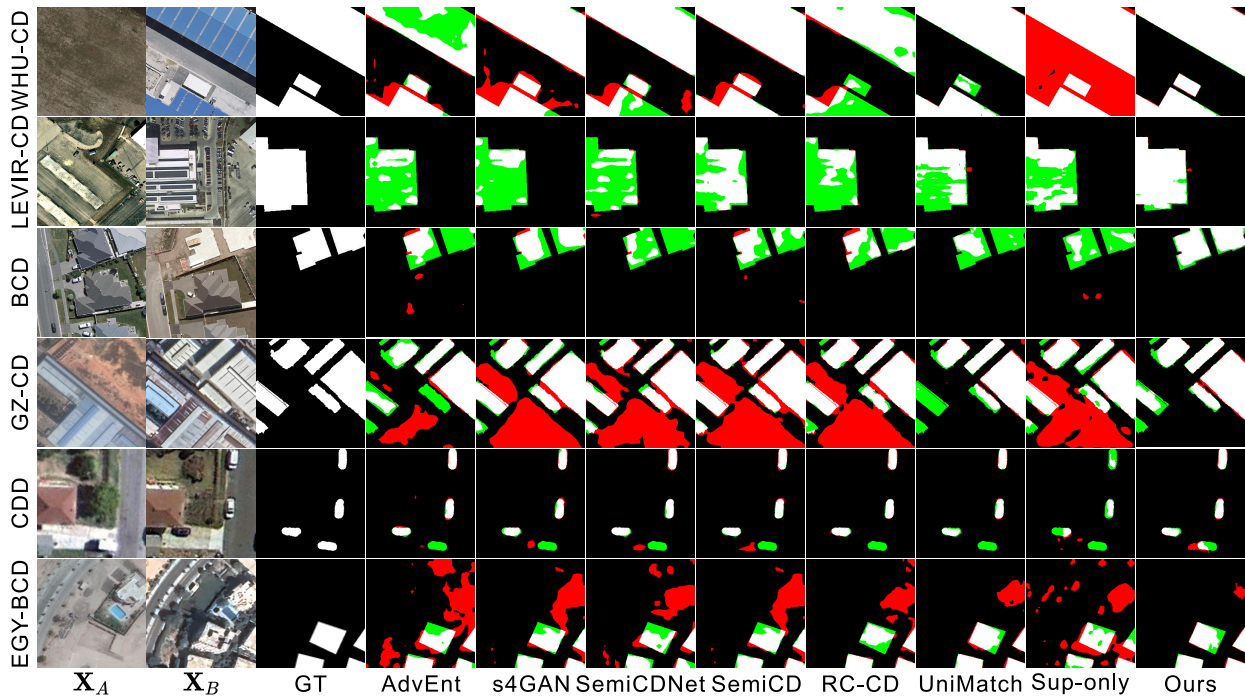


Fig. 3. Detection results of different methods on six CD datasets at the 5% labeled training ratio. Different colors are used for a better view, i.e., white for true positive, black for true negative, red for false positive, and green for false negative.

level and feature-level perturbations contribute to performance enhancement, and their combined utilization further improves performance. ② A comparison between “Feature + Image” and “Ours(FP(d1))” reveals that incorporating the gate mechanism helps distinguish challenging samples, reducing training difficulty and improving performance. ③ Under the “With Gate” condition, contrasting “FP(d4)”, “FP(d1,d4)”, and “Ours(FP(d1))” indicates that disturbing deep-level features can introduce excessive disruptions, increasing training complexity. Disturbing only the shallow-level features appears more robust than disturbing the deep-level features. ④ Under the “With Gate” condition, “Ours(FP(d1))” employs ResNet50 as the backbone. In comparison with the approach based on “ResNet101”, it is observed that with a limited number of labels, the performance of the ResNet50-based is slightly better than that of the ResNet101-based. As the number of labels increases, the performance of ResNet101-based surpasses that of the ResNet50-based.

TABLE IV
ABLATION STUDY ON WHU-CD DATASET.

	Method	5%		10%		20%		40%	
		IoU	OA	IoU	OA	IoU	OA	IoU	OA
Without Gate	Sup-only	41.4	96.36	55.0	97.28	49.3	96.98	65.6	98.26
	Feature	68.0	98.49	73.9	98.80	74.3	98.77	82.0	99.21
	Image	77.4	99.03	80.0	99.14	77.5	98.97	82.2	99.22
	Feature + Image	81.7	99.24	81.6	99.21	79.2	99.07	84.8	99.35
With Gate	FP(d4)	79.4	99.13	78.0	99.03	82.9	99.25	83.4	99.28
	FP(d1, d4)	78.5	99.08	81.3	99.20	79.4	99.07	84.4	99.33
	Ours(FP(d1))	83.0	99.30	82.8	99.28	84.2	99.31	85.4	99.37
	ResNet101	82.6	99.28	82.3	99.24	82.1	99.21	85.7	99.39

Sensitivity of the gate mechanism. We apply the optimal threshold on WHU-CD due to space limitations. The experi-

mental results are shown in Fig 4. High ratio lead to unstable training as more samples are perturbed, while low ratio may miss perturbation opportunities. Median threshold strikes a balance.

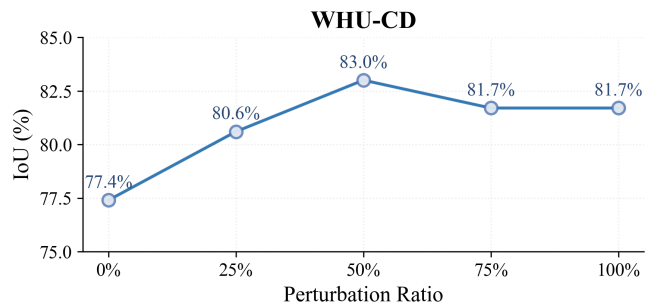


Fig. 4. Performance comparison with different perturbation ratios under 5% labeled training data on WHU-CD dataset.

IV. CONCLUSION

In this work, we introduce a novel gate-guided two-level perturbation consistency regularization-based SSCD method. This approach ensures image-level strong-to-weak consistency and feature-level perturbation consistency, enabling efficient utilization of a large amount of unlabeled data. Moreover, we design a gate module to intelligently access the need of feature perturbations. Extensive experiments on six benchmark datasets validate the effectiveness and superiority of our proposed method. In the future, we will further explore enabling the network to autonomously determine the most effective perturbation strategies tailored to various data scenarios.

REFERENCES

- [1] A. Singh, "Review article digital change detection techniques using remotely-sensed data," *International Journal of Remote Sensing*, vol. 10, no. 6, pp. 989–1003, 1989.
- [2] Y. You, J. Cao, and W. Zhou, "A survey of change detection methods based on remote sensing images for multi-source and multi-objective scenarios," *Remote Sensing*, vol. 12, no. 15, p. 2460, 2020.
- [3] G. Cheng, Y. Huang, X. Li, S. Lyu, Z. Xu, H. Zhao, Q. Zhao, and S. Xiang, "Change detection methods for remote sensing in the last decade: A comprehensive review," *Remote Sensing*, vol. 16, no. 13, p. 2355, 2024.
- [4] S. H. Khan, X. He, F. Porikli, and M. Bennamoun, "Forest change detection in incomplete satellite images with deep neural networks," *IEEE Transactions on Geoscience and Remote Sensing*, vol. 55, no. 9, pp. 5407–5423, 2017.
- [5] T.-H. Lin and C.-H. Lin, "Hyperspectral change detection using semi-supervised graph neural network and convex deep learning," *IEEE Transactions on Geoscience and Remote Sensing*, 2023.
- [6] J. Z. Xu, W. Lu, Z. Li, P. Khaitan, and V. Zaytseva, "Building damage detection in satellite imagery using convolutional neural networks," *arXiv preprint arXiv:1910.06444*, 2019.
- [7] H. Chen and Z. Shi, "A spatial-temporal attention-based method and a new dataset for remote sensing image change detection," *Remote Sensing*, vol. 12, no. 10, p. 1662, 2020.
- [8] S. Hafner, Y. Ban, and A. Nascetti, "Urban change detection using a dual-task siamese network and semi-supervised learning," in *IGARSS 2022 - 2022 IEEE International Geoscience and Remote Sensing Symposium*, 2022, pp. 1071–1074.
- [9] T.-H. Vu, H. Jain, M. Bucher, M. Cord, and P. Pérez, "Advent: Adversarial entropy minimization for domain adaptation in semantic segmentation," in *2019 IEEE/CVF Conference on Computer Vision and Pattern Recognition (CVPR)*, 2019, pp. 2517–2526.
- [10] D. Peng, L. Bruzzone, Y. Zhang, H. Guan, H. Ding, and X. Huang, "Semicdnet: A semisupervised convolutional neural network for change detection in high resolution remote-sensing images," *IEEE Transactions on Geoscience and Remote Sensing*, vol. 59, no. 7, pp. 5891–5906, 2020.
- [11] S. Yang, S. Hou, Y. Zhang, H. Wang, and X. Ma, "Change detection of high-resolution remote sensing image based on semi-supervised segmentation and adversarial learning," in *IGARSS 2022-2022 IEEE International Geoscience and Remote Sensing Symposium*, 2022, pp. 1055–1058.
- [12] J.-X. Wang, T. Li, S.-B. Chen, J. Tang, B. Luo, and R. C. Wilson, "Reliable contrastive learning for semi-supervised change detection in remote sensing images," *IEEE Transactions on Geoscience and Remote Sensing*, vol. 60, pp. 1–13, 2022.
- [13] L. Kondmann, S. Saha, and X. X. Zhu, "Semisiroc: Semisupervised change detection with optical imagery and an unsupervised teacher model," *IEEE Journal of Selected Topics in Applied Earth Observations and Remote Sensing*, vol. 16, pp. 3879–3891, 2023.
- [14] X. Hou, Y. Bai, Y. Xie, H. Ge, Y. Li, C. Shang, and Q. Shen, "Deep collaborative learning with class-rebalancing for semi-supervised change detection in sar images," *Knowledge-Based Systems*, vol. 264, p. 110281, 2023.
- [15] W. G. C. Bandara and V. M. Patel, "Revisiting consistency regularization for semi-supervised change detection in remote sensing images," *arXiv preprint arXiv:2204.08454*, 2022.
- [16] C. Sun, J. Wu, H. Chen, and C. Du, "Semisanet: A semi-supervised high-resolution remote sensing image change detection model using siamese networks with graph attention," *Remote Sensing*, vol. 14, no. 12, p. 2801, 2022.
- [17] Q. Ding, Z. Shao, X. Huang, X. Feng, O. Altan, and B. Hu, "Consistency-guided lightweight network for semi-supervised binary change detection of buildings in remote sensing images," *GIScience & Remote Sensing*, vol. 60, no. 1, p. 2257980, 2023.
- [18] C. Sun, H. Chen, C. Du, and N. Jing, "Semibuildingchange: A semi-supervised high-resolution remote sensing image building change detection method with a pseudo bi-temporal data generator," *IEEE Transactions on Geoscience and Remote Sensing*, 2023.
- [19] Z. Mao, X. Tong, and Z. Luo, "Semi-supervised remote sensing image change detection using mean teacher model for constructing pseudo-labels," in *ICASSP 2023-2023 IEEE International Conference on Acoustics, Speech and Signal Processing (ICASSP)*, 2023, pp. 1–5.
- [20] K. Sohn, D. Berthelot, N. Carlini, Z. Zhang, H. Zhang, C. A. Raffel, E. D. Cubuk, A. Kurakin, and C.-L. Li, "Fixmatch: Simplifying semi-supervised learning with consistency and confidence," *Advances in Neural Information Processing Systems*, vol. 33, pp. 596–608, 2020.
- [21] Q. Shu, J. Pan, Z. Zhang, and M. Wang, "Mtcnet: Multitask consistency network with single temporal supervision for semi-supervised building change detection," *International Journal of Applied Earth Observation and Geoinformation*, vol. 115, p. 103110, 2022.
- [22] X. Zhang, X. Huang, and J. Li, "Joint self-training and rebalanced consistency learning for semi-supervised change detection," *IEEE Transactions on Geoscience and Remote Sensing*, 2023.
- [23] L. Yang, L. Qi, L. Feng, W. Zhang, and Y. Shi, "Revisiting weak-to-strong consistency in semi-supervised semantic segmentation," in *2023 IEEE/CVF Conference on Computer Vision and Pattern Recognition (CVPR)*, 2023, pp. 7236–7246.
- [24] S. Ji, S. Wei, and M. Lu, "Fully convolutional networks for multisource building extraction from an open aerial and satellite imagery data set," *IEEE Transactions on Geoscience and Remote Sensing*, vol. 57, no. 1, pp. 574–586, 2018.
- [25] J. Kim, Y. Min, D. Kim, G. Lee, J. Seo, K. Ryoo, and S. Kim, "Con-match: Semi-supervised learning with confidence-guided consistency regularization," in *Proceedings of the European conference on computer vision (ECCV)*. Springer, 2022, pp. 674–690.
- [26] D. Berthelot, N. Carlini, E. D. Cubuk, A. Kurakin, K. Sohn, H. Zhang, and C. Raffel, "Remixmatch: Semi-supervised learning with distribution alignment and augmentation anchoring," *arXiv preprint arXiv:1911.09785*, 2019.
- [27] S. Yun, D. Han, S. J. Oh, S. Chun, J. Choe, and Y. Yoo, "Cutmix: Regularization strategy to train strong classifiers with localizable features," in *2019 IEEE/CVF International Conference on Computer Vision (ICCV)*, 2019, pp. 6023–6032.
- [28] Y. Ouali, C. Hudelot, and M. Tami, "Semi-supervised semantic segmentation with cross-consistency training," in *2020 IEEE/CVF Conference on Computer Vision and Pattern Recognition (CVPR)*, 2020, pp. 12 674–12 684.
- [29] T. Miyato, S.-i. Maeda, M. Koyama, and S. Ishii, "Virtual adversarial training: a regularization method for supervised and semi-supervised learning," *IEEE Transactions on Pattern Analysis and Machine Intelligence*, vol. 41, no. 8, pp. 1979–1993, 2018.
- [30] K. He, X. Zhang, S. Ren, and J. Sun, "Deep residual learning for image recognition," in *2016 IEEE Conference on Computer Vision and Pattern Recognition (CVPR)*, 2016, pp. 770–778.
- [31] L.-C. Chen, Y. Zhu, G. Papandreou, F. Schroff, and H. Adam, "Encoder-decoder with atrous separable convolution for semantic image segmentation," in *Proceedings of the European conference on computer vision (ECCV)*, 2018, pp. 801–818.
- [32] S. Mittal, M. Tatarchenko, and T. Brox, "Semi-supervised semantic segmentation with high-and low-level consistency," *IEEE Transactions on Pattern Analysis and Machine Intelligence*, vol. 43, no. 4, pp. 1369–1379, 2019.
- [33] S. Holail, T. Saleh, X. Xiao, and D. Li, "Afde-net: Building change detection using attention-based feature differential enhancement for satellite imagery," *IEEE Geoscience and Remote Sensing Letters*, vol. 20, pp. 1–5, 2023.
- [34] M. Lebedev, Y. V. Vizilter, O. Vygolov, V. A. Knyaz, and A. Y. Rubis, "Change detection in remote sensing images using conditional adversarial networks," *The International Archives of the Photogrammetry, Remote Sensing and Spatial Information Sciences*, vol. 42, pp. 565–571, 2018.